Technical University of Denmark

DTU

A regional and nonstationary model for partial duration series of extreme rainfall

Gregersen, Ida Bülow; Madsen, Henrik; Rosbjerg, Dan; Arnbjerg-Nielsen, Karsten

Link back to DTU Orbit

DTU Library
Technical Information Center of Denmark

A REGIONAL AND NON-STATIONARY MODEL FOR PARTIAL DURATION SERIES OF EXTREME RAINFALL

Ida Bülow Gregersen

Department of Environmental Engineering, Technical University of Denmark, Bygningstorvet, Building 115, DK-2800 Lyngby

Presently working at:

Ramboll, Hannemanns Allé 53, DK-2300 Kbh S

idbg@env.dtu.dk

Henrik Madsen

DHI, Agern Alle 5, DK-2970 Hørsholm

hem@dhigroup.com

Dan Rosbjerg

Department of Environmental Engineering, Technical University of Denmark, Bygningstorvet, Building 115, DK-2800 Lyngby

daro@env.dtu.dk

Karsten Arnbjerg-Nielsen

Department of Environmental Engineering, Technical University of Denmark, Bygningstorvet, Building 115, DK-2800 Lyngby

karn@env.dtu.dk

ABSTRACT

Regional extreme value models for estimation of extreme rainfall intensities are widely applied, but their underlying assumption of stationarity is challenged. Many recent studies show that the rainfall extremes worldwide exhibit a non-stationary behavior. This paper presents a spatio-temporal model of extreme rainfall. The framework is built on a Partial Duration Series approach with a non-stationary, regional threshold value. The model is based on Generalized Linear Regression solved

31 by Generalized Estimation Equations. It allows a spatial correlation between the stations in the

32 network and accounts furthermore for variable observation periods at each station and in each year.

33 Marginal regional and temporal regression models solved by Generalized Least Squares are used to

34 validate and discuss the results of the full spatio-temporal model.

35 The model is applied on data from a large Danish rain gauge network for four durations ranging

36 from 10 minutes to 24 hours. The observation period differs between stations, and the number of

37 stations with more than 10 years of observations has increased over the years. A spatio-temporal

38 model for the threshold is suggested, applying the Mean Annual Precipitation and time as the

39 explanatory variables in the regional and temporal domain, respectively. Further analysis of Partial

40 Duration Series with non-stationary and regional thresholds shows that the mean exceedances also

41 exhibit a significant variation in space and time for some rainfall durations, while the shape

42 parameter is found to be constant.

1 INTRODUCTION

44 Non-stationary extreme value frameworks for estimation of design rainfall or design floods have

45 received increased attention along with the numerous reports of observed trends in extreme rainfall

46 and flood statistics [e.g. *Min et al.,* 2011; *Westra et al.,* 2013; *Sun et al.,* 2015; *Madsen et al.,* In

47 Review]. Regional extreme value models for extreme rainfall have been applied in many countries,

48 e.g. Denmark, Norway, UK, Canada and Australia [*Madsen et al.,* 2002; *Dyrrdal et al.*, 2014;

49 *Fowler and Kilsby,* 2003; *Wallis et al.*, 2007; *Haddad et al.,* 2011]. Several frameworks for regional

50 modelling exist, built on different principles. The most traditional is the index-flood model, which

51 became widely applied after the advancement of the regional L-moment approach by *Hosking and*

52 *Wallis* [1993]. In this framework the uncertainty of the estimated at-site design events is reduced by

53 the estimation of regional extreme value distribution (EVD) parameters from a homogenous region.

54 The index-flood model was originally applied for annual maxima extremes in a stationary setting.

55 Later advancements include an extension to Peak over Threshold (POT) data [*Haddad et al.*, 2011;

56 *Madsen and Rosbjerg*, 1997] based on Generalized Least Squares (GLS) estimation procedures

57 [*Stedinger and Tasker* 1985] where the variability of the EVD parameters is modelled by regional

58 covariates. This framework accounts for both at-site sampling uncertainty and spatial dependencies

59 between the observations at different sites. Regarding non-stationarity of the parameters of the

60 EVD, *Gregersen et al.* [*2013a*] presented a model for the spatio-temporal variation of the number of

61 extreme events building on the framework of Generalized Linear Models (GLM), while *Roth et al.*

62 [2012] used the POT-threshold as the index variable and allowed it to vary in both time and space.

63 As discussed by *Kyselý et al.* [2010], a non-stationary threshold is crucial when having a non-

64 uniform distribution of extreme events over the observation period, because the otherwise variable

65 intensity of the Poisson process will violate the asymptotic properties of the POT model. Suitable

66 non-stationary threshold models are often found by quantile regression [*Kyselý et al.*, 2010; *Roth et*

67 *al.*, 2012].

68

69 A drawback of the regression based index flood method is that inferences are made on statistics

70 derived from the observations and not from the observations directly [*Renard, 2011*]. Some authors

71 prefer another type of regional model based on hierarchical principles, which overcomes this

72 problem. In the hierarchical model prior distributions are defined for each of the parameters in the

73 EVD [e.g. *Aryal et al.*, 2009; *Dyrrdal et al.*, 2014; *Ghosh and Mallick*, 2011; *Heaton et al.*, 2011;

74 *Renard*, 2011; *Sun et al.*, 2015]. From here there are numerous possibilities with regard to the

75 specific model formulation and the parameter estimation algorithms. Hierarchical extreme value

76 models are often solved by sampling algorithms like the Markov Chain Monte Carlo method

77 [*Cooley*, 2007; *Dyrrdal et al.*, 2014; *Ghosh and Mallick*, 2011; *Renard*, 2011]. Recently, an

78 alternative approach based on the max-stable framework solved by composite likelihood has gained

79 attention [*Thibaud et al.,* 2013; *Westra and Sisson,* 2011]. *Roth et al.* [2012] also applied composite

80 likelihood but on an index-flood model derived from POT data. Like the hierarchical model, both

81 models can include regional and temporal variability in a dataset with a spatial correlation structure.

82 Regarding regional variations in the parameters some authors use a Kriging technique [*Aryal et al.,*

83 2009], a trivariate Gaussian process with an exponential, distance depending covariance function

84 [e.g. *Cooley,* 2007; *Heaton et al.,* 2011] or a combination of the latter and regression to regional

85 covariates [e.g. *Dyrrdal et al.,* 2014; *Ghosh and Mallick,* 2011; *Renard,* 2011). Temporal variations

86 are also assessed together with their influence on the regionalization [e.g. *Aryal et al.,* 2009; *Ghosh*

87 *and Mallick,* 2011; *Heaton et al.,* 2011; *Renard,* 2006; *Roth et al.,* 2012; *Sun et al.,* 2015; *Westra*

88 *and Sisson,* 2011]. Some of these studies include spatial dependencies between the observations at

89 different locations. This can be numerically and theoretically difficult, but with a dense network the

90 uncertainty of the model parameters is greatly underestimated, if the joint probability of observing a

91 given extreme at several sites is disregarded [*Roth et al.,* 2012; *Westra and Sisson,* 2011]. Joint

92 probabilities can be described by copula functions, which therefore can be included in the

93 hierarchical models to account for the spatial dependencies [*Ghosh and Mallick,* 2011; *Renard,*

94 2011]. *Sun et al.* [2015] developed a description applicable for a network of flow measurement

95 stations along a branched river. In a max-stable process for extreme rainfall, spatial dependence on

96 the data level is accounted for by a storm profile model, which is naturally incorporated in the

97 framework [*Thibaud et al.,* 2013; *Westra and Sisson,* 2011].

98

99 The salient point in all above-mentioned non-stationary approaches is the description of the spatial

100 dependencies and, most importantly, the assumptions enforced to solve the complicated equation

101　structure it entails. This becomes particularly difficult for a model based on POT data from a rain

102　gauge network with a varying number of annually active stations, though *Ghosh and Mallick*

103　[2011], *Roth et al.* [2012] and *Thibaud et al.* [2013] show very promising results.

104　The purpose of this paper is to extend the regression based index flood model solved by GLS

105　[*Madsen and Rosbjerg,* 1997] that is currently applied in Denmark for regional estimation of

106　extreme rainfall [*Madsen et al.,* 2002; 2009; In Review) to include a temporal dimension. The

107　procedure developed comprises a GLM solved by the Generalized Estimation Equations (GEE)

108　approach applied by *Gregersen et al.* [2013a] but now extended to more parameters of the EVD.

109　Preliminary analyzes of the temporal and regional variations are performed by marginal models as

110　in *Gregersen et al.* [2013a]. The first analysis aims to formulate a non-stationary threshold model.

111　The quantile regression approach is inapplicable due to the independence criteria traditionally

112　applied for this type of rainfall data (see Section 3 for details). Subsequently, the threshold model is

113　validated and applied. Finally, regional and temporal variations of EVD parameters are assessed.

114　All calculations are performed for four different rainfall durations relevant for urban drainage

115　design.

2 METHODOLOGY

2.1 PARTIAL DURATION SERIES AND REGIONAL ESTIMATION OF EXTREME RAINFALL

118　The extreme value analysis follows the theory of Partial Duration Series (PDS) where the annual

119　number of extreme events (N) is assumed to follow a Poisson distribution with rate parameter (λ),

$$P\{N = n\} = \frac{\lambda^n}{n!}e^{-\lambda}, \quad N = 0, 1, 2\ldots \tag{1}$$

120　and the magnitude of the extreme events (z) is assumed to follow a Generalized Pareto Distribution

121　(GPD) with a location (β), a scale (α) and a shape (κ) parameter

$$F(z) = P\{Z \le z\} = 1 - \left(1 + \kappa \frac{z - \beta}{\alpha}\right)^{1/\kappa} \tag{2}$$

122   [*Coles,* 2001; *Rosbjerg et al.,* 1992]. When sampling the extreme events from a time series, the PDS

123   approach offers two censoring methods [*Mikkelsen et al.*, 1995]. In type 1 censoring, the threshold

124   (z_0) over which an event is considered as extreme is pre-fixed. The method is also known as Peak

125   over Threshold [*Coles,* 2001]. In this case z_0 replaces β in the GPD in Eq. (2). All other parameters

126   in Eq. (1) and Eq. (2) are estimated from the dataset. In type 2 censoring, λ, and thereby the total

127   number of extremes during the observation period, is pre-fixed. In this case all parameters in Eq. (2)

128   are estimated from the dataset.

129

130   The extreme events in the PDS are required to be independent [*Coles,* 2001]. In the literature there

131   are at least two common ways of ensuring this. Many studies perform a declustering procedure

132   based only on the time span between the extreme events [e.g. *Ghosh and Mallick,* 2011; *Roth et al.,*

133   2012], while *Madsen et al.* [2002] performed an event-based separation using information on the

134   dry-weather period. This method is particularly useful for tipping bucket rainfall measurements,

135   where the observations are stored as events (see Section 3).

136

137   The procedures from *Madsen et al.,* [2002] are applied here. Therefore, two rainfall events are

138   independent if the dry weather period between them is longer than or equal to the analyzed rainfall

139   duration. This event-based separation procedure is performed prior to the PDS approach and is

140   therefore valid independent of the selected PDS censoring. Available for the extreme value analysis

141   is therefore a series of independent events (*Y*) represented by the maximum mean intensity of the

142   event (*y*) for a given duration, and the start and termination time (t_{start} , t_{end}) for the event for each

6

143   site, *s* (see Madsen et al. [2002] for definition of event-based maximum mean intensity). The dataset

144   includes in total K stations; $s = 1, 2 \ldots K$. Furthermore the dataset includes M years of

145   measurements; $i = 1, 2 \ldots M$. Not all sites have measurements during the entire period; therefore K

146   varies from year to year $s_i = 1, 2 \ldots K_i$ while M varies from site to site $i_s = 1, 2 \ldots M_s$. In addition, $l_{i,s}$

147   denotes number of observation days in year *i* at site *s*.

148   In the regional model by *Madsen et al.,* [2002, 2009, In Review] type 1 censoring is applied using

149   the same z_0 at all sites in the region. λ of the Poisson distribution is estimated from

$$\widehat{\lambda}_s = \frac{N_s}{l_s} \tag{3}$$

150   where N_s is the total number of exceedances in the full observation period l_s at site *s*. The GPD

151   parameters are estimated by the method of L-moments [*Hosking,* 1990]. From the first L-moment

152   (b_0), which corresponds to the mean, and the second L-moment (b_1) the following parameters are

153   defined

$$\widehat{\mu} = b_0 \quad \text{and} \quad \widehat{L}_{cv} = \frac{b_1}{b_0} \tag{4}$$

154   κ of the GPD is directly related to L_{cv}

$$\widehat{\kappa} = \frac{1}{\widehat{L}_{cv}} - 2 \tag{5}$$

155   while $\widehat{\alpha}$ of the GPD is estimated from $\widehat{\mu}$ and $\widehat{L}_{CV}$ [*Hosking,* 1990]. Madsen *et al.* (2002, 2009,

156   In Review) showed that λ and μ exhibit significant regional patterns, while L_{CV} and thereby κ is

157   homogeneous over the region. This gives the following estimate of a regional T-year event

$$\widehat{z}_{T,s} = z_0 + \widehat{\mu}_s \frac{1 + \widehat{\kappa}_R}{\widehat{\kappa}_R} \left[1 - \left(\frac{1}{\widehat{\lambda}_s T} \right)^{\widehat{\kappa}_R} \right] \tag{6}$$

158   where index *s* refers to a site-specific estimate and *R* to a regional estimate. As discussed in the

159   introduction, a clear shortcoming of this model is that temporal variations are not accounted for.

160   The first step pursued in this paper is to develop a spatio-temporal model for β, which can be

161   applied on the series of independent rainfall events. With a method to describe and evaluate this

162   variability, it is possible to define a model for z_0, which will ensure that λ does not exhibit

163   significant variations over time and space. The second step is to apply the threshold model and

164   analyze the remaining variability in the GDP parameters.

165   *2.1.1 A SPATIO-TEMPORAL MODEL FOR β*

166   A PDS is defined from Y using type 2 censoring, PDS_2. The rate parameter of the Poisson

167   distribution is prefixed ($\lambda = 4$ events/year). The choice of rate parameter is based on experience

168   from earlier studies (*Madsen et al.,* [2002, 2009]).]. Since the aim is to capture the regional and

169   temporal variation, the censoring is performed for each year individually. From PDS_2 β is

170   estimated for each year, i, and each site, s, as the minimum exceedance in a year. A regression

171   model is constructed for $\hat{\beta}_{i,s}$ evaluating both regional and temporal variations, following the

172   procedures described in Section 2.2 and 2.3.

173   *2.1.2 TYPE 1 CENSORING APPLYING A TIME-DEPENDENT AND REGIONAL THRESHOLD*

174   The model for β found in the first step is applied as a deterministic model for z_0 . On this basis a

175   new PDS is defined from Y using type 1 censoring with a pre-fixed z_0 that varies in time and space.

176   In the following this PDS is denoted PDS_1. The properties of PDS_1 is validated by assessing the

177   variability of λ. λ is a random variable in the model, but λ should not exhibit any significant

178   variations in time and space, since this variability is explained by the variation in z_0. Therefore a

179   regional estimate of λ can be applied. μ and L_{CV} are also estimated from PDS_1 and their regional and

180   temporal variation is assessed following the procedures described in Section 2.2 and 2.3.

181

182   In each of the two steps marginal models are obtained by averaging over either time i or space s.

183   After this a full spatio-temporal model is developed based on GLM solved by GEE as in *Gregersen*

184   *et al.* [2013a]. In both the full model and the marginal models knowledge on the correlation

185   between the rain gauge stations is required.

2.2 MARGINAL MODELS

187   The general procedures behind the marginal GLS models are similar for all the analyzed GDP

188   parameters: β from PDS_2 and λ, μ and L_{CV} from PDS_1. The following description of the

189   methodology applied to assess the variation in space and time, respectively, focuses on β. When

190   relevant, conditions that make the approach different for one of the other variables are highlighted.

2.2.1 MARGINAL MODEL FOR VARIATION IN SPACE

192   Site specific estimates of β are obtained from an average over all years of observation at the site

$$\beta_s = \frac{\sum_{i=1}^{M_s} \beta_{i,s}}{M_s} \tag{7}$$

193   The average of a given quantity asymptotically follows a normal distribution, so analyzes of β_s can

194   be based on linear regression. GLS is applied to include a possible spatial correlation between the

195   observations and a weighting that reflects the sampling uncertainty, which for a specific site s is

196   related to the total period of observation l_s or the total number of observations n_s at that location.

197

198   The following regression model is tested

$$\beta_s = XB_{\beta s} + \varepsilon_\Sigma \tag{8}$$

199   where X is a matrix of regional covariates, $\mathbf{B}_{\beta s}$ is the regression parameters, and Σ is the variance-

200   covariance matrix of the model residuals ε. The following structure of Σ is assumed in the GLS

201   model of β_s

$$\boldsymbol{\Sigma} = \begin{bmatrix} \sigma_{\varepsilon 1}^2 + \sigma_\delta^2 & \sigma_{\varepsilon 1}\sigma_{\varepsilon 2}\rho_{12} & \cdots & & & \sigma_{\varepsilon 1}\sigma_{\varepsilon K}\rho_{1K} \\ \sigma_{\varepsilon 2}\sigma_{\varepsilon 1}\rho_{21} & \sigma_{\varepsilon 2}^2 + \sigma_\delta^2 & & & & \sigma_{\varepsilon 2}\sigma_{\varepsilon K}\rho_{2K} \\ \vdots & & \ddots & \sigma_{\varepsilon s}\sigma_{\varepsilon k}\rho_{sk} & & \vdots \\ & & \sigma_{\varepsilon k}\sigma_{\varepsilon s}\rho_{ks} & & & \\ \sigma_{\varepsilon K}\sigma_{\varepsilon 1}\rho_{K1} & \sigma_{\varepsilon K}\sigma_{\varepsilon 2}\rho_{K2} & \cdots & & & \sigma_{\varepsilon K}^2 + \sigma_\delta^2 \end{bmatrix} \tag{9}$$

202   In the matrix σ_ε represents the sampling uncertainty, σ_δ the residual uncertainty in the regression

203   model, and ρ the spatial correlation. σ_δ is assumed to be unknown and is estimated along with the

204   other variables in the regression model. The estimation of ρ is described in the following section,

205   while σ_ε is a function of the variance of $\hat{\beta}_s$ and l_s.

206

207   A description of σ_ε for each of the analyzed extreme value statistics is given in Appendix A.1. For

208   β_s, σ_ε is estimated as

$$\hat{\sigma}_{\varepsilon s}^2 = \frac{c}{l_s} \qquad \text{where} \qquad c = \frac{1}{K}\sum_{s=1}^{K}\left(\frac{\sum_{i=1}^{M_s}\left(\beta_{i,s} - \overline{\beta}_s\right)^2}{M_s - 1}\right) \tag{10}$$

209   where $\overline{\beta}_s$ is the average over all sites.

210

211   A similar procedure is applied for λ_s and μ_s, while for L_{CVs} Monte Carlo simulations are applied (see

212   Appendix A.1). All estimation procedures of σ_ε assume stationarity over time.

213

214   For comparison, ordinary linear regression (OLS) is also applied for the estimation of $\mathbf{B}_{\beta s}$. In OLS

215   both sampling uncertainty and spatial correlation are disregarded. Furthermore, the statistical

216   significance of the explanatory variables is evaluated by a t-test on the ratio between the regression

217   slope and its standard deviation. A similar quantity can be estimated for GLS, but here it is also

218   important to assess σ_δ both in the regression model and in an intercept model, i.e. where only the

219   intercept is included in Eq.(8). If σ_δ is close to zero in the intercept model or negative, all variability

220   is accounted for by the estimated sampling uncertainty, and explanatory variables cannot contribute

221   to a further reduction. Likewise, the value of σ_δ in the regression model can be used to assess the

222   amount of unexplained variability.

223   2.2.2 CORRELATION BETWEEN RAIN GAUGE STATIONS

224   A framework that estimates the spatial dependence between extreme rainfall events at individual

225   rain gauge stations has been developed by *Mikkelsen et al.* [1996] for PDS. It is applied to obtain a

226   robust, regional estimation of the correlation structure to be used in Σ, see Eq. (9). To ensure this,

227   the spatial correlation, ρ, of the GPD parameters is first estimated from the data, and subsequently,

228   described by a parametric correlation model. For further discussion, see *Madsen and Rosbjerg*

229   [1997].

230   For β and λ, ρ is estimated from annual time series of $\beta_{i,s}$ for all pairs of stations. If a rain gauge has

231   long periods of malfunction during a year, it will affect the estimate of $\beta_{i,s}$ and hence ρ. Therefore

232   individual station years are removed from the analysis if the total observation period in a given year

233   is less than 300 days. For μ a method is used, which pairs events that in a physical sense can be

234   regarded concurrent. This is done for each pair of stations, based on t_{start} of the events combined

235   with a lag time, which accounts for the travelling time of the weather systems. For details the reader

236   is referred to *Gregersen et al.* [2013b] and *Mikkelsen et al.* [1996]. Finally, the correlogram is

237   estimated by averaging ρ over distance intervals and subsequently described by an exponential

238   model.

239   2.2.3 MARGINAL MODEL FOR VARIATION IN TIME

240   Annual estimates of β are obtained from an average over all stations. Due to the correlation between

241   the stations in the network a weighted average is applied so the influence of station clusters with

242   similar properties is reduced

$$\beta_i = \frac{\sum_{s=1}^{K_i} \beta_{i,s} w_s}{K_i} \tag{11}$$

243   The applied weights (w_s) are estimated for each station as one minus the average correlation

244   coefficient between the given station and all other stations in the network. High weights are given to

245   stations with low average correlation, and all weights sum to one.

246

247   As in Section 2.2.1, analyzes of β_i can be based on linear regression, where GLS is applied to

248   include a weighting that reflects the sampling uncertainty. Temporal correlation is discarded, as it is

249   assumed that the estimates of β_i are independent from year to year. The sampling uncertainty of β_i

250   relates to the total period of observation l_i or the total number of observations at the active stations

251   K_i in year i.

252

253   The following regression model is tested

$$\beta_i = \boldsymbol{X}\boldsymbol{B}_{\beta i} + \boldsymbol{\varepsilon}_{\Sigma} \tag{12}$$

254   where the following structure of Σ is assumed in the GLS model of β_i

$$\boldsymbol{\Sigma} = \begin{bmatrix} \sigma_{\varepsilon 1}^2 + \sigma_{\delta}^2 & 0 & \cdots & \\ 0 & \sigma_{\varepsilon 2}^2 + \sigma_{\delta}^2 & & \\ \vdots & & \ddots & \\ & & & \sigma_{\varepsilon K}^2 + \sigma_{\delta}^2 \end{bmatrix} \tag{13}$$

255   In the matrix σ_{ε} represents the sampling uncertainty and σ_{δ} the residual uncertainty in the regression

256   model. σ_{δ} is assumed to be unknown and is estimated along with the other variables in the

257   regression model. σ_{ε} is estimated as

12

$$\hat{\sigma}_{\varepsilon i}^2 = \frac{c}{l_i} \qquad \text{where} \qquad c = \frac{1}{M}\sum_{i=1}^{M}\left(\frac{\sum_{s=1}^{K_i}\left(\beta_{i,s}-\overline{\beta_i}\right)^2}{K_{i,\mathit{eff}}-1}\right) \tag{14}$$

258   where $\overline{\beta_i}$ is the average over all sites.

259

260   The correlation between the stations, which was accounted for in the estimation of β_i, also affects

261   the variance of β_i as the amount of independent information in the dataset is reduced. This is

262   accounted for by estimating the effective number of stations each year using [*Madsen et al.,* 1994]

$$K_{i,\mathit{eff}} = K_i\left(1+\left(K_i-1\right)\overline{\rho_i}\right)^{-1} \tag{15}$$

263   where $\overline{\rho_i}$ is the average correlation between stations active in the given year.

264

265   A description of σ_ε for λ_i and μ_i is given in Appendix A.2. For comparison, ordinary linear

266   regression (OLS) is also applied for the estimation of $\mathbf{B}_{\beta i}$, where both sampling uncertainty and

267   spatial correlation are disregarded.

268   2.3 SPATIO-TEMPORAL MODELS

269   The concept of GLM solved by GEE was applied by *Gregersen et al.* [2013a] for the number of

270   extreme events, *N*, which follows a Poisson distribution. GLM applies to all distributions within the

271   exponential family and also allows for the use of a link function (*g*) mapping the modelled variable

272   ($\beta_{i,s}$) and the linear relation to the explanatory variable (*X*) given by the regression parameters ($\mathbf{B}_\eta$)

$$\boldsymbol{\eta} = \boldsymbol{X}\boldsymbol{B}_\eta + \boldsymbol{\varepsilon}_\Sigma \qquad \text{where} \qquad g(\boldsymbol{\beta}_{i,s}) = \boldsymbol{\eta} \tag{16}$$

273   The link function can ensure that restrictions on the sample space are fulfilled, i.e. for $\beta_{i,s}$, $\lambda_{i,s}$ and

274    $\mu_{i,s}$ only positive estimates are meaningful. The identity link, a log link and an inverse link are

275   among the commonly used functions [*Faraway,* 2006].

13

276   Several of the probability distributions from the PDS and GLS frameworks belong to the

277   exponential family, i.e. the Gaussian distribution, the Poisson distribution [*Gregersen et al.,* 2013a]

278   and the Gamma distribution, of which the exponential distribution is a special case. The choice of

279   distribution in the GLM framework can be based on prior knowledge on the process generating the

280   data or from standard evaluations of the data and the model residuals. GLM is solved by maximum

281   likelihood procedures. The log-likehood is derived from the density function, where the link

282   function is included, before the values of B_η that optimize the likelihood are estimated, either

283   directly or by an iteration scheme, *Gregersen et al.* [2013a].

284

285   With the GEE extension [*Halekoh et al.,* 2006; *Hardin and Hilbe,* 2003] the GLM framework can

286   account for spatial correlation between stations and a weight ($w_{i,s}$) reflecting how many days during

287   a specific year a given station has been active. *Gregersen et al.* [2013a] showed how the correlation

288   matrix is included in the estimation equations for a Poisson model. The division of the observed

289   variance into sampling uncertainty and model uncertainty done by the GLS model cannot be

290   implemented in the same manner here, as σ_ε in the marginal regional model is estimated from the

291   temporal variability and vice versa. GLM with the GEE extension is solved by maximum likelihood

292   procedures.

293

294   All calculations are performed using the statistical software R, using the packages 'geepack'

295   [*Halekoh et al.,* 2006; *Højsgaard et al.,* 2014], 'doBy' [*Højsgaard and Halekoh,* 2014] and 'lmom'

296   [*Hosking,* 2014].

297   # 3 DATA AND CASE STUDY

298   Rainfall series from 83 high-resolution tipping buckets are analyzed. The network was established

299   in 1979 and has expanded since then, while a few stations are closed. All stations included in the

300   present analysis have more than 10 years of measurements. When periods of rain gauge malfunction

301   have been taken into account, the total dataset corresponds to 1881 station-years. The data

302   resolution is one minute and 0.2 mm. Rainfall durations of 10, 60, 180 and 1440 minutes are

303   analyzed.

304

305   The network is operated by the Danish Water Pollution Committee and the Danish Meteorological

306   Institute (DMI), who also conduct the quality-control. Data from this network has since 1998 been

307   applied for estimation of design intensities for urban drainage design [*Madsen et al.,* 2002], and the

308   applied model has been updated twice [*Madsen et al.,* 2009; In Review]. Analyzes of temporal

309   variation of extreme rainfall by *Gregersen et al.* [2013a; 2013b] were also based on data from this

310   network.

311

312   The most recent model for regional variation of extreme rainfall over Denmark applied two

313   explanatory variables [*Madsen et al.,* In Review] derived from Climate Grid Denmark (CGD). Here

314   λ varies with the Mean Annual Precipitation (MAP) [mm], while μ varies with the mean value of

315   daily rainfall extremes (μ_{CGD}) [mm]. CGD is a gridded dataset of daily precipitation provided by

316   DMI. It has a spatial resolution of 10x10 km^2 and covers the period 1989-2010 [*Scharling,* 2012].

317   The grid values are estimated from point measurements obtained from the regional network of daily

318   precipitation stations owned by DMI using an inverse distance weighting method. The documented

319   link between λ and MAP is exploited in the present study; as we aim at having a constant λ over

320   space z_0 must vary with MAP.

321

322 *Gregersen et al.* [2013a] tested several teleconnections as explanatory variables for the temporal

323 variation in *N,* while *Gregersen et al.* [2014] concluded that the natural variability induced by these

324 teleconnections can appear as short term temporal trends that last a few decades.. As the aim of the

325 present study is to evaluate the influence of ==non-stationary== data on a regional extreme value model,

326 *time* is used as the only temporal explanatory variable. In this relation *time* is defined as the number

327 of years since 1978. A year is defined as the calendar year January-December. The majority of

328 extreme rainfall events occur in the period May-October [*Gregersen et al.,* 2013b; *Pedersen et al.,*

329 2012]. Therefore, with the use of the calendar year estimated extreme rainfall statistics are

330 independent from year to year; a necessary assumption as mentioned in Section 2.2.3.

331 # 4 RESULTS

332 ## 4.1 SPATIO-TEMPORAL MODELS FOR β

333 From type 2 censoring PDS_2 is defined as the fourth largest independent event at each site for each

334 year. Subsequently, β is estimated and the regional and temporal variability are evaluated by the

335 two marginal models and the full spatio-temporal model. All models take into account the spatial

336 dependence between the PDS series, which is estimated first.

337 ### 4.1.1 CORRELATION BETWEEN RAIN GAUGE STATIONS

338 The spatial correlation structure, applied in the three models of β is given in Figure 1. The shape of

339 the correlogram depends on the rainfall duration. In general the correlation decreases with distance,

340 but stations far away remains correlated. The shape of the curves corresponds well with the findings

341 of *Gregersen et al.* [2013a] and *Madsen et al.* [In Review].

342 ### 4.1.2 MARGINAL REGIONAL MODEL FOR β

343 Initial analyzes of the intercept model (not shown) confirm that $\hat{\sigma}_\delta^2$ is positive for all durations.

344 Hence regional variability exists, which potentially can be reduced by the introduction of

345 explanatory variables. The following regression model is analyzed by GLS and for means of

346 comparison by OLS:

$$\beta_s = a + b \cdot MAP + \varepsilon_\Sigma \tag{17}$$

347 The estimated model parameters are given in Table 1, while the observations and the modelled

348 relation are shown in Figure 2 for all four durations. Accounting for spatial correlation and

349 sampling uncertainty change the regression parameters and their uncertainty slightly (see Table 1).

350 An influence of *MAP* is suggested for very long rainfall (1440 min) durations.

351

352 As discussed in *Madsen et al.* [In Review], it is expected that the variability over time, when not

353 accounted for, is introducing an additional uncertainty in the regional model. The length of

354 observation period differs between stations. An effect of this can be seen from Figure 2 where

355 stations, which have been active approximately during the entire period from 1979 to 2012, are

356 marked with black. The variability in this subset of stations is remarkably lower than the variability

357 of the entire sample. In Section 4.1.4, it is shown that the spatio-tempor   al model accounts for

358 this.

359 4.1.3 MARGINAL TEMPORAL MODEL FOR β

360 For β the spatial correlation is relatively high, also for sites separated by long distances (see Section

361 4.1.1). This has a substantial effect on the sampling uncertainty, because $K_{i,eff}$, despite the large

362 number of stations in the network, is very small, s   ee Eq.(15).   Still, initial analyzes of the

363 intercept model (not shown) confirm that $\hat{\sigma}_\delta^2$ is positive for 10 and 60 minutes and is greatly

364 reduced by the introduction of temporal regressors. *Gregersen* [2015] showed that when λ is

365 analyzed in a similar manner $\hat{\sigma}_\delta^2$ is positive for all durations. Therefore the analysis is continued for

366 all durations and the following regression model is analyzed by GLS:

$$\beta_i = a + c \cdot time + \varepsilon_\Sigma \tag{18}$$

367 Again, parameter estimates from OLS regression are also assessed. Estimated model parameters are

368 given in Table 2, while the observations and the modelled relations are shown in Figure 3 for all

369 four durations. For all rainfall durations β_i increases over time. A comparison between OLS and

370 GLS (not included) shows that the standard errors on the regression slopes for 10 and 60 minutes

371 increase slightly when the sampling uncertainty is taken into account. Besides that the other

372 parameter estimates are almost identical for the two methods.

373 4.1.4 THE FULL SPATIAL AND TEMPORAL MODEL FOR β

374 The two marginal models show variability in both domains and thereby a need for the formulation

375 of a spatio-temporal model. The following regression model is analyzed by GLM-GEE

$$\eta_{i,s} = a + b \cdot MAP + c \cdot time + \varepsilon_\Sigma \quad \text{where} \quad g(\beta_{i,s}) = \eta_{i,s} \tag{19}$$

376 It must be evaluated which underlying probability distribution is best suited to describe $\beta_{i,s}$. A

377 histogram combined with a kernel-approximation of the density function shows no large deviations

378 from a Gaussian distribution, see Figure 4a. Furthermore, different distributions and link functions

379 were tested in the GLM-GEE model. It was found that the parameter estimates varied little and that

380 the residuals showed approximately the same behavior independent of the choice of model, see

381 Figure 4b and Figure 4c. For the convenience of direct comparison with the parameter estimates

382 from the two marginal GLS models, the subsequent analysis is based on a GLM-GEE model with a

383 Gaussian distribution and an identity link function.

384

385   Table 3 shows the results for all four rainfall durations using the most complex GLM-GEE model

386   with both weights and correlation. It has been evaluated how the assumption on the structure of the

387   residuals (weights and correlation) affects the parameter estimates and their significance (not

388   shown). The conclusion depends on the rainfall durations, but in general the variation of the

389   parameter estimates and their significance are not substantially different from the variation between

390   the OLS and the GLS estimates in the marginal models.

391

392   For all durations the full model with weights and correlation reduces the parameter uncertainty on b

393   compared to the marginal regional GLS model, see Table 3. This leads to a significant correlation to

394   *MAP* for all durations but 60 minutes. The estimate of b has decreased for 10 min, but increased for

395   180 and 1440 minutes. This corresponds well to the behaviour reported by *Madsen et al.* [In

396   Review]. All in all it is confirmed that when the assumption of stationarity is not fulfilled the

397   overall model uncertainty increases with the available information. The spatio-temporal model

398   solves this issue. The estimates of c are also slightly different from the estimates of the marginal

399   temporal model as an effect of the variability explained by *MAP* and the covariance between the

400   parameter estimates.

401   4.2 TYPE 1 CENSORING APPLYING A SPATIO-TEMPORAL THRESHOLD

402   The spatio-temporal model of β is applied as a deterministic model for z_0 to define a new PDS from

403   Y using type 1 censoring (PDS_1). When z_0 varies in time and space, λ must not exhibit any

404   significant variations over time and space. For a duration of 60 minutes a regression to *MAP* is

405   included even though it is non-significant.

406

407   From PDS_1 the GPD parameters from Eq.(6) are estimated, and their variation over time and space

408   is assessed including the spatial correlation structure.

4.2.1 CORRELATION BETWEEN RAIN GAUGE STATIONS

The spatial correlation structure for λ and μ is given in Figure 5 and Figure 6, respectively. The shape of the correlogram depends on the rainfall duration. In general, the correlation decreases with distance, and this happens quickly for μ, while for λ stations far away remain correlated. A comparison with the findings by *Madsen et al.* [In Review] (not shown) indicates that when a non-stationary threshold is applied the correlation decreases slightly.

4.2.2 VARIATIONS OF λ OVER TIME AND SPACE

The two following marginal regression models are analyzed

$$\lambda_s = a + b \cdot MAP + \varepsilon_\Sigma \tag{20}$$
$$\lambda_i = a + c \cdot time + \varepsilon_\Sigma \tag{21}$$

to test that the application of the non-stationary and regional z_0 leads to constant λ over time and space. This is confirmed. Furthermore, the variability of all data points and a subset of data points representing the stations with long records (black dots) are comparable, see Figure 7. This is not the case when the temporal variability is not accounted for, see Figure 2. Station outliers are observed for all durations. Two stations from suburbs west of Copenhagen recur as outliers. As they both are approved by the quality control, they are retained in the dataset. One of the stations was closed in 1995.

The following regression model is analyzed by GLM-GEE to estimate the constant λ and the uncertainty on the estimate:

$$\eta_{i,s} = a + \text{offset}\left(\log\left(l_{i,s}\right)\right) + \varepsilon_\Sigma \quad \text{where} \quad \log(N_{i,s}) = \eta_{i,s} \tag{22}$$

$N_{i,s}$ is assumed to follow a Poisson distribution, while the variability of $\lambda_{i,s}$ can be modelled by including the observation period in the model as an offset. A Poisson model with a log-link function is applied following the approach by *Gregersen et al.* [2013a]. The results are given in Table 4.

429   The scale of the Poisson distribution is reported to evaluate if $N_{i,s}$ shows overdispersion; values

430   close to one indicate that this is not the case. The results are applied for estimation of design

431   intensities in Section 4.3.

432   4.2.3 VARIATIONS OF μ OVER TIME AND SPACE

433   Initial analyzes of the marginal intercept models (not shown) confirm that $\hat{\sigma}_\delta^2$ is positive for all

434   durations in both the temporal and regional domain. The following two marginal regression models

435   are analyzed

$$\mu_s = a + b \cdot \mu_{CGD} + \varepsilon_\Sigma \tag{23}$$
$$\mu_i = a + c \cdot time + \varepsilon_\Sigma \tag{24}$$

436   The regression between μ and *time* is positive, see Figure 8, and significant for all durations but

437   1440 minutes, see Table 5. The regression between μ and μ_{CGD} is positive, see Figure 9, and

438   significant on a 10% confidence level for 10, 180 and 1440 minutes, see Table 5. However, residual

439   analysis (not shown) indicates that the marginal model for the variation in space is too simple,

440   because the variance seemingly increases with the mean for both 60 and 180 minutes. This tendency

441   can also be seen directly from Figure 9. The full spatio-temporal variation is described by the

442   following model and analyzed by GLM-GEE

$$\eta_{i,s} = a + b \cdot \mu_{CGD} + c \cdot time + \varepsilon_\Sigma \quad \text{where} \quad g(\mu_{i,s}) = \eta_{i,s} \tag{25}$$

443   A histogram of $\mu_{i,s}$ shows a distribution with a positive skew, which is suggesting the use of a

444   Gamma distribution in the GLM-GEE, see Figure 10. A Gamma model is also suitable if the

445   variance of the residuals increases with the mean. As potential link functions for the Gamma model,

446   a log link and an inverse link are considered. Evaluations show that the significance of the

447   regression parameters are almost identical for the two different link functions (not shown), but

448   residual analysis suggests that the increase of the variance is captured best by the inverse link, see

449   Figure 10. Therefore, the inverse link is applied. The estimated model parameters are given in Table

450   5. These show a difference between the significance of the regression coefficients in the marginal

451   models and the full model. The reason is that the underlying model assumptions differ as the

452   gamma model can account for an increase of the variance. This probably leads to the found

453   difference in significance of μ_{CGD} for 10 and 180 minutes.

454   4.2.4 VARIATIONS OF L_{CV} OVER TIME AND SPACE

455   L_{cv} exhibits no apparent variation over space and time (not shown). Estimation of the heterogeneity

456   measure from *Hosking and Wallis* [1993] confirms that the parameter can be regarded as

457   homogenous. L_{cv} is estimated following the method from *Madsen et al.* [2002], and results are given

458   in Table 6.

459   4.3 ESTIMATION OF DESIGN INTENSITIES

460   Based on the results from the preceding sections the following model for the estimation of T-year

461   events is suggested

$$z_{T,i,s} = z_{0,i,s} + \mu_{i,s} \frac{1+\kappa}{\kappa} \left[1 - \left(\frac{1}{\lambda T} \right)^{\kappa} \right] \tag{26}$$

462    $z_{0i,s}$ is fixed in the applied PDS procedure and hence by definition not uncertain. All other

463   parameters estimated from *PDS₁* are predicted from the regional and temporal covariates, if these

464   are found significant in the full model. By use of Eq.(26) the 10-year event ($z_{10i,s}$) is predicted for

465   two locations in Denmark and compared to the results from *Madsen et al.* [In Review], see Table 7.

466   The uncertainty on $z_{10i,s}$ is approximated by a second order Taylor expansion of Eq.(26) [*Madsen et*

467   *al.,* 2002].

468

469   The temporal development of the 10-year event is strongest for 10, 60 and 180 minutes, where both

470   λ and μ has a non-stationary component. For these three durations the estimate from *Madsen et al.*

471 [In Review] lies in between the two years for which predictions are made (see Table 7). This

472 corresponds well with the data that the model by *Madsen et al.* [In Review] is built on. For 1440

473 min the variability is strongest in the regional domain as both λ and μ has a regional component. A

474 small temporal variability is seen due to the temporal development in λ. Comparing the estimated

475 uncertainties on the 10-year events, with the results from *Madsen et al.* [In Review] it is seen, that

476 the proposed regional and non-stationary model for PDS successfully eliminates the uncertainty

477 introduced when the assumption of stationarity is not fulfilled.

478 ## 5 DISCUSSION

479 The identified model is primarily used for explorative purposes. Over the last 15 years the urban

480 drainage engineering community has experienced increases of recommended design intensities of

481 extreme precipitation of the 'present' (i.e. 'stationary') climate that by far exceeds the anticipated

482 changes due to emissions of greenhouse gasses in any of the future scenarios foreseen by the

483 climate change communities. The purpose of the model has been to validate that this process has

484 taken place and to separate the process into a regional and a temporal component. Future work will

485 focus on separating the temporal component into processes that can be validated and predicted,

486 thereby distinguishing between observed dynamics in the past, present, and future, and anticipated

487 climatic changes due to emissions of greenhouse gasses.

488

489 Using the identified model it is in principle possible to obtain design values for infrastructure by

490 extrapolating into the future and consider e.g. the maximum design values over the expected

491 technical lifetime and using that in the design process. Procedures for making such projections

492 (although for different variables than precipitation) are described in e.g. *Larsen et al.* [2003] and

493 *Arnbjerg-Nielsen* [2011]. However, as pointed out in a commentary by *Montanari and*

494   *Koutsoyiannis* [2014] the practical application of statistical models with a time-dependent

495   component can be questionable, which is why process-based models are preferable. This study has

496   not addressed the physical processes which could lie behind the temporal variation. Several studies

497   indicate that large scale climatic variables may influence extreme rainfall [e.g. *Sun et al.,* 2014;

498   *Willems* 2013], but even when the large scale physical drivers are known, several challenges still

499   remain; first to predict their future states, secondly to select which state to apply when choosing the

500   design intensity. Hence, the present study demonstrates the non-stationary model using time as

501   covariate. Since all model applications are uncertain outside the range of the input variables we do

502   not recommend to use the identified model in its present form for estimating design intensities for

503   the future.

504

505   As pointed out by *Willems* [2013] and *Gregersen et al.* [2014] there may be some cyclical processes

506   occurring with low frequency that, once understood, can serve as a more suitable co-variate in the

507   model. This would enable projections into the future that are more trust-worthy if future states of

508   these co-variates can be obtained. If climate drivers replace the variable *time*, this will have an

509   effect on the model residuals and the estimated uncertainty on the design intensities. This potential

510   reduction in uncertainty is, based on earlier work using teleconnections, assumed to be minor in

511   comparison to the difference between including and not including a temporal variable [*Gregersen et*

512   *al.,* 2013a].

513   # 6 CONCLUSION

514   In conclusion, the suggested GLM-GEE procedure is shown to be highly qualified for modelling

515   spatio-temporal variability in β, λ and μ and thereby for the construction of a non-stationary regional

516   extreme value model, which can be used for the estimation of urban design rainfall.

518   The dataset is first assessed by type 2 PDS censoring to find a suitable model for the threshold. The

519   model is subsequently used in type 1 PDS censoring to ensure that the occurrences of extreme

520   events are identically distributed over the sample period. These PDS are analyzed for a temporal

521   and regional development in the mean exceedances and the shape parameter. The GLM-GEE

522   framework can include a spatial correlation between the measurements and a weight reflecting a

523   possible difference in the observation period. However, it is not possible to include the sampling

524   uncertainty of the observation directly. If the magnitude of the sampling uncertainty is equal to the

525   total variability of the data, there is no reason to search for regional or temporal explanatory

526   variables. It is therefore recommended to assess the marginal development in space and time, and

527   the magnitude of sampling uncertainty in both domains before the full spatio-temporal model is

528   applied. Thereby, model overfitting and underestimation of uncertainty are avoided. A GLS

529   framework is well suited for evaluation of the marginal models.

530   Rainfall duration of 10, 60, 180 and 1440 minutes were analyzed. For β, a spatio-temporal model is

531   suggested, applying the Mean Annual Precipitation and time as the explanatory variables in the

532   regional and temporal domain, respectively. This threshold model ensures a constant λ. A

533   significant temporal increase in the mean of the extreme exceedences was found for 10, 60, 180

534   minutes, while for 1440 minutes a significant regional variability was found. No significant

535   temporal or regional variability of the shape parameter was found, and hence a regionally constant

536   estimate was applied.

537

538   *Westra and Sisson* [2011] and *Roth et al.* [2012] accessed the effect of spatial correlation on the

539   identification of temporal trends by different methods. A comparison of methods is highly relevant.

540   The next step is to evaluate the differences and similarities of the proposed model and the methods

541 of *Ghosh and Mallick* [2011], *Roth et al.* [2012] and *Thibaud et al.* [2013], in terms of spatial

542 correlation, significance of spatial and temporal variables, and prediction of urban design

543 intensities.

544

545 **Acknowledgements**

553

7 REFERENCES

Arnbjerg-Nielsen K. (2011). Past, present, and future design of urban drainage systems with focus on Danish experiences. *Water Science and Technology*, 63(3), 527-535. DOI: 10.2166/wst.2011.253

Aryal, S. K., B. C. Bates, E. P. Campbell, Y. Li, M. J. Palmer and N. R. Viney (2009). Characterizing and modeling temporal and spatial trends in rainfall extremes. *Journal of Hydrometeorology*. 10(1), 241-253. DOI: 10.1175/2008JHM1007.1

Coles, S. (2001). An introduction to statistical modeling of extreme values. Springer. London, UK.

Cooley, D., D. Nychka and P. Naveau (2007). Bayesian spatial modeling of extreme precipitation return levels. *Journal of the American Statistical Association*. 102(479), 824-840.

Dyrrdal, A. V., Lenkoski, A., Thorarinsdottir, T. L., and Stordal, F. (2014). Bayesian hierarchical modeling of extreme hourly precipitation in Norway. *Environmetrics*. DOI: 10.1002/env.2301

Faraway, J.J. (2006). Extending the linear model with R: Generalized linear, mixed effects and nonparametric regression models. Chapman and Hall/CRC. Boca Raton, Florida, U.S.

Fowler, H. J. and C. G. Kilsby (2003). A regional frequency analysis of United Kingdom extreme rainfall from 1961 to 2000. *International Journal of Climatology*. 23(11), 1313-1334. DOI: 10.1002/joc.943

Frich, P., S. Rosenørn, H. Madsen and Jensen, J.J. (1997). Observed precipitation in Denmark, 1961–1990. Technical report 97-8. Danish Meteorological Institute, Ministry of Transport. Copenhagen, Denmark.

Ghosh, S. and B. K. Mallick (2011). A hierarchical Bayesian spatio-temporal model for extreme precipitation events. *Environmetrics*. 22(2), 192-204. DOI: 10.1002/env.1043

Gregersen, I. B., H. Madsen, D. Rosbjerg and K. Arnbjerg-Nielsen (2013a). A spatial and nonstationary model for the frequency of extreme rainfall events. *Water Resources Research*. 49(1), 127-136.

Gregersen, I. B., H. J. D. Sørup, H. Madsen, D. Rosbjerg, P. S. Mikkelsen and K. Arnbjerg-Nielsen, (2013b). Assessing future climatic changes of rainfall extremes at small spatio-temporal scales. *Climatic Change*. 118(3-4), 783-797. DOI: 10.1007/s10584-012-0669-0

Gregersen, I. B., H. Madsen, D. Rosbjerg and K. Arnbjerg-Nielsen (2014). Long term variations of extreme rainfall in Denmark and southern Sweden. *Climate Dynamics*. 44(11-12), 3155-3169. DOI: 10.1007/s00382-014-2276-4

585 Gregersen, I. B. (2015). Past, present and future variations of extreme rainfall in Denmark, Ph.D.
586   Thesis. Department of Environmental Engineering, Technical University of Denmark, Kgs.
587   Lyngby, Denmark.

588 Haddad, K., A. Rahman and Green, J. (2011). Design rainfall estimation in Australia: a case study
589   using L moments and Generalized Least Squares Regression. *Stochastic Environmental*
590   *Research and Risk Assessment*. 25(6), 815-825. DOI: 10.1007/s00477-010-0443-7

591 Halekoh, U., S. Hojsgaard and Yan, J. (2006). The R Package geepack for Generalized Estimating
592   Equations. *Journal of Statistical Software*. 15(2), 1-11.

593 Hardin, J.W. and J.M. Hilbe (2003). Generalized estimating equations. Chapman & Hall/CRC.
594   Boca Raton, Florida, U.S.

595 Heaton, M. J., M. Katzfuss, S. Ramachandar, K. Pedings, E. Gilleland, E. Mannshardt-Shamseldin
596   and R. L. Smith (2011). Spatio-temporal models for large-scale indicators of extreme weather.
597   *Environmetrics*. 22(3), 294-303. DOI: 10.1002/env.1050

598 Hosking, J. R. M. (1990). L-moments: analysis and estimation of distributions using linear
599   combinations of order statistics. *Journal of the Royal Statistical Society.Series B*
600   *(Methodological)*. 52(1), 105-124.

601 Hosking, J. R. M. and J. R. Wallis (1993). Some Statistics Useful in Regional Frequency-Analysis.
602   *Water Resources Research*. 29(2), 271-281.

603 Hosking, J. R. M. (2014). Package 'lmom', February 20 2015, version 2.5. Available from:
604   http://cran.r-project.org/web/packages/lmom/lmom.pdf . Assessed: July 2016.

605 Højsgaard, S and U. Halekoh (2014). Package 'doBy', March 31 2016, version 4.5-15. Available
606   from: http://cran.r-project.org/web/packages/doBy/doBy.pdf . Assessed: July 2016.

607 Højsgaard, S, U. Halekoh and J. Yan (2014). Package 'geepack', July 2016, version 1.2-0.2
608   Available from: http://cran.r-project.org/web/packages/geepack/geepack.pdf . Assessed: July
609   2016.

610 Kyselý, J., J. Picek and R. Beranova (2010). Estimating extremes in climate change simulations
611   using the peaks-over-threshold method with a non-stationary threshold. *Global and Planetary*
612   *Change*. 72(1-2), 55-68. DOI: 10.1016/j.gloplacha.2010.03.006

613 Larsen, O.D., Moelgaard, C. and Kampmann, J. (2003). Flooding of the Copenhagen Metro,
614   Denmark. *Structural Engineering International*, 13(4), 231-234.

615 Madsen, H., D. Rosbjerg and P. Harremoës (1994). PDS-modelling and regional Bayesian
616   estimation of extreme rainfalls, *Nordic Hydrology*. 25(4), 279-300.

Madsen, H. and D. Rosbjerg (1997). Generalized least squares and empirical Bayes estimation in regional partial duration series index-flood modeling. *Water Resources Research*. 33(4), 771-781.

Madsen, H., P. S. Mikkelsen, D. Rosbjerg and P. Harremoes (2002). Regional estimation of rainfall intensity-duration-frequency curves using generalized least squares regression of partial duration series statistics. *Water Resources Research*. 38(11).

Madsen, H., K. Arnbjerg-Nielsen and P. S. Mikkelsen (2009). Update of regional intensity-duration-frequency curves in Denmark: Tendency towards increased storm intensities. *Atmospheric Research*. 92(3), 343-349. DOI: 10.1016/j.atmosres.2009.01.013

Madsen, H., D. Lawrence, M. Lang, M. Martinkova, T.R. Kjeldsen (2014). Review of trend analysis and climate change projections of extreme precipitations and floods in Europe. *Journal of Hydrology*. 519(PD), 3634-3650. DOI: 10.1016/j.jhydrol.2014.11.003

Madsen, H., I. B. Gregersen, D. Rosbjerg and K. Arnbjerg-Nielsen (In Review). Regional frequency analysis of short duration rainfall extremes using gridded daily rainfall data as co-variate. Submitted to *Water Science and Technology*.

Mikkelsen, P. S., H. Madsen, D. Rosbjerg, and P. Harremoes (1996). Properties of extreme point rainfall .3. Identification of spatial inter-site correlation structure. *Atmospheric Research*. 40(1), 77-98. DOI: 10.1016/0169-8095(95)00026-7

Mikkelsen, P. S., P. Harremoes and D. Rosbjerg (1995). Properties of extreme point rainfall .2. Parametric data interpretation and regional uncertainty assessment. *Atmospheric Research*. 37(1995), 287-304. DOI: 10.1016/0169-8095(94)00054-H

Min, S. K., X. Zhang, F. W. Zwiers and Hegerl, G. C. (2011). Human contribution to more-intense precipitation extremes. *Nature*. 470(7334), 376-379. DOI: 10.1038/nature09763

Montanari, A. and D. Koutsoyiannis, (2014). Modelling and mitigating natural hazards: Stationarity is immortal!. *Water Resources Research*. 50(12), 9748-9756. DOI: 10.1002/2014WR016092

Pedersen, A. N., P. S. Mikkelsen and K. Arnbjerg-Nielsen (2012). Climate change-induced impacts on urban flood risk influenced by concurrent hazards. *Journal of Flood Risk Management*. 5(3), 203-214. DOI: 10.1111/j.1753-318x.2012.01139.x

Renard, B. (2011). A Bayesian hierarchical approach to regional frequency analysis. *Water Resources Research*. 47(11).

Rosbjerg, D., H. Madsen, and P. F. Rasmussen (1992). Prediction in Partial Duration Series with generalized Pareto distributed exceedances. *Water Resources Research*. 28(11), 3001-3010.

Roth, M., T. Buishand, G. Jongbloed, A. Tank and J. van Zanten (2012). A regional peaks-over-threshold model in a nonstationary climate. *Water Resources Research*. 48(11).

651 Scharling, M. (2012). Climate Grid Denmark - Dataset of use in research and education - Daily and
652   monthly values 1989-2010. Technical report 12-10. Danish Meteorological Institute, Ministry of
653   Climate and Energy. Copenhagen, Denmark.

654 Stedinger, J. R. and G. D. Tasker (1985). Regional Hydrologic Analysis .1. Ordinary, weighted, and
655   generalized least-squares compared. *Water Resources Research*. 21(9), 1421-1432.

656 Sun, X., M. Thyer, B. Renard and M. Lang (2014). A general regional frequency analysis
657   framework for quantifying local-scale climate effects: A case study of ENSO effects on
658   Southeast Queensland rainfall. *Journal of Hydrology*. 512(2014), 6586-6601. DOI:
659   10.1016/j.jhydrol.2014.02.025

660 Sun, X., U. Lall, B. Merz and N.V. Dung (2015). Hierarchical Bayesian clustering for nonstationary
661   flood frequency analysis: Application to trends of annual maximum flow in Germany. *Water
662   Resources Research*. 51(8), 6586-6601.

663 Thibaud, E., R. Mutzner and A. Davison (2013). Threshold modeling of extreme spatial rainfall.
664   *Water Resources Research*. 49(8), 4633-4644.

665 Wallis, J., M. Schaefer, B. Barker and G. Taylor (2007). Regional precipitation-frequency analysis
666   and spatial mapping for 24-hour and 2-hour durations for Washington State. *Hydrology and
667   Earth System Sciences*. 11(1), 415-442.

668 Westra, S. and S. A. Sisson (2011). Detection of non-stationarity in precipitation extremes using a
669   max-stable process model. *Journal of Hydrology*. 406(1-2), 119-128. DOI:
670   10.1016/j.jhydrol.2011.06.014

671 Westra, S., L. V. Alexander and F. W. Zwiers (2013). Global increasing trends in annual maximum
672   daily precipitation. *Journal of Climate*. 26(11), 3904-3918. DOI: 10.1175/JCLI-D-12-00502.1

673 Willems, P. (2013) Multidecadal oscillatory behaviour of rainfall extremes in Europe. *Climatic
674   Change*. 120(4), 931-944. DOI: 10.1007/s10584-013-0837-x

675 APPENDICES

676 A.1 SAMPLING UNCERTAINTY FOR THE MARGINAL REGIONAL MODEL

677 The applied procedure for estimation of the sample uncertainty on β_s, λ_s, μ_s and L_{CVs} are reviewed

678 below, starting with β_s. Unless specifically stated the procedures follow *Madsen and Rosbjerg*

679 [1997].

680

681 For any of the of the four GPD parameters the GLS procedure requires, that the at-site estimate of

682 the sampling uncertainty ($\hat{\sigma}_{\varepsilon s}$) is nearly independent of the estimated parameter ($\hat{\theta}_S$) [*Madsen and*

683 *Rosbjerg,* 1997]. *Madsen and Rosbjerg* [1997] and *Madsen et al.* [2002] therefore applied an

684 estimation procedure based on sample estimates of the population parameters.

685

686 A given site s has M_s observations of β; one for each year where the station has been active. On this

687 basis the mean and variance of β are estimated for each site, and subsequently for the entire

688 population by averaging over all K sites. A site specific estimation of the sampling uncertainty is

689 obtained by accounting for the actual observation period at the site, l_s:

$$\widehat{\sigma}_{\varepsilon s}^2 = \frac{c}{l_s} \quad \text{where} \quad c = \frac{1}{K}\sum_{s=1}^{K}\left(\frac{\sum_{i=1}^{M_s}\left(\beta_{i,s} - \overline{\beta_{0s}}\right)^2}{M_s - 1} \right) \tag{1A}$$

690 where $\overline{\beta_s}$ is the average over all sites.
691
692 The sampling uncertainty of λ_s is estimated from a procedure identical to the one described for β_s. In

693 *Madsen and Rosbjerg* [1997] and *Madsen et al.* [2002] it is utilized that λ_s is the rate parameter of

694 the Poisson distribution and hence the variance equals the mean. To ensure consistency between the

695 sampling uncertainty estimates in the marginal regional and temporal model the approach from

696 equation 1A is preferred. In the marginal temporal model correlation between stations is accounted

697 for in the estimation of the variance. This procedure cannot be applied if the variance is assumed

698 equal to the mean.

699

700 The sampling uncertainty of μ_s is estimated from a procedure similar to the one described for β_s. A

701 given site s has n_s observations of extreme rainfall with intensity y. n_s is indirectly related to how

702 many years the station has been active. The mean and variance are estimated for each site, and

703   subsequently for the entire population by averaging over all K sites. A site specific estimation of the

704   sampling uncertainty is obtained by accounting for the number of observations at the site, n_s:

$$\widehat{\sigma}_{\varepsilon s}^2 = \frac{c}{n_s} \quad \text{where} \quad c = \frac{1}{K} \sum_{s=1}^{K} \left(\frac{\sum_{j=1}^{n_s} \left(y_j - \mu_s \right)^2}{n_s - 1} \right) \tag{2A}$$

705   where μ_s is the average over all sites.

706

707   For higher moments the estimation of the sampling uncertainty cannot be based on the population

708   parameters if the independence criteria should be fulfilled. Simulations are therefore required. A

709   four parameter kappa distribution is suitable for this purpose because of its flexibility [*Madsen et*

710   *al.,* 2002].

711

712   The sampling uncertainty of L_{CVs} is estimated from Monto Carlo simulation using the kappa

713   distribution with parameters estimated from regional estimates of the first four L-moments. In total

714   500 series with $\overline{n}_s$ observations are generated from this distribution, and applied for estimation of

715     $\mathrm{Var}(L_{cv})_{mc}$. Here $\overline{n}_s$ is the average number of events over all sites. A site specific estimation of the

716   sample uncertainty is obtained accounting for the ratio between $\overline{n}_s$ and the actual number of

717   observations at the site, n_s:

$$\widehat{\sigma}_{\varepsilon s}^2 = \frac{c}{n_s} \quad \text{where} \quad c = \mathrm{Var}(L_{cv})_{mc} \cdot \overline{n}_s \tag{3A}$$

718   A.2 SAMPLING UNCERTAINTY FOR THE MARGINAL TEMPORAL MODEL

719   The applied procedure for estimation of the sampling uncertainty of β_i, λ_i and μ_i is reviewed below,

720   starting with β_i.

721

722　　The marginal temporal GLS model is similar to the marginal regional GLS model, just averaging

723　　over the regional domain instead. The considerations regarding appropriate estimators of the

724　　sampling uncertainty given for the regional GLS model therefore applies. With the important

725　　difference that the estimate of sampling uncertainty is affected by the correlation between sites,

726　　which reduces the amount of information in the data set and increases the sample estimate of the

727　　population variance.

728

729　　For β a given year i has K_i observations of β, one for each station active that year. On this basis the

730　　mean and variance are estimated for each year.　The variance is corrected for the correlation

731　　between stations by dividing the sum of squared differences with $K_{i,eff}$, which is estimated from:

$$K_{i,eff} = K_i \left(1 + \left(K_i - 1 \right) \overline{\rho_i} \right)^{-1} \tag{4A}$$

732　　where $\overline{\rho_i}$ is the average correlation between stations active in the given year. The mean and

733　　variance are estimated by averaging over all M years. A site specific estimation of the sampling

734　　uncertainty is obtained by accounting for the actual number of active stations in the given year and

735　　their breakdown periods, i.e. the number of station years l_i:

$$\hat{\sigma}_{\varepsilon i}^2 = \frac{c}{l_i} \quad \text{where} \quad c = \frac{1}{M} \sum_{i=1}^{M} \left(\frac{\sum_{s=1}^{K_i} \left(\beta_{i,s} - \overline{\beta_{0i}} \right)^2}{K_{i,eff} - 1} \right) \tag{5A}$$

736　　The sampling uncertainty of λ_i is estimated from a procedure identical to the one described for β_i.

737

738　　The sampling uncertainty of μ_i is also estimated from a procedure similar to the one described for

739　　β_i. A given year i has n_i observations of extreme rainfall with intensity y. On this basis the mean and

740　　variance are estimated for each year.　The variance must again be corrected for the correlation

741　　between stations. However, as one site often has more than one observation and at-site observations

742　　are uncorrelated $n_{i,eff}$ is estimated as:

$$n_{i,\text{eff}} = \overline{n}_i K_{\text{eff}} \tag{6A}$$

743 where $\overline{\rho}_i$ is the average correlation between stations active in the given year and $K_{i,\text{eff}}$ is given by

744 (4A). The mean and variance are estimated by averaging over all M years. A site specific estimation

745 of the sampling uncertainty is obtained by accounting for the actual number of active observations

746 that year:

$$\widehat{\sigma}_{\varepsilon i}^2 = \frac{c}{n_i} \quad \text{where} \quad c = \frac{1}{M} \sum_{i=1}^{M} \left(\frac{\sum_{j=1}^{n_s} \left(y_j - \mu_i \right)^2}{n_{i,\text{eff}} - 1} \right) \tag{7A}$$

747

All figures with caption. Figure
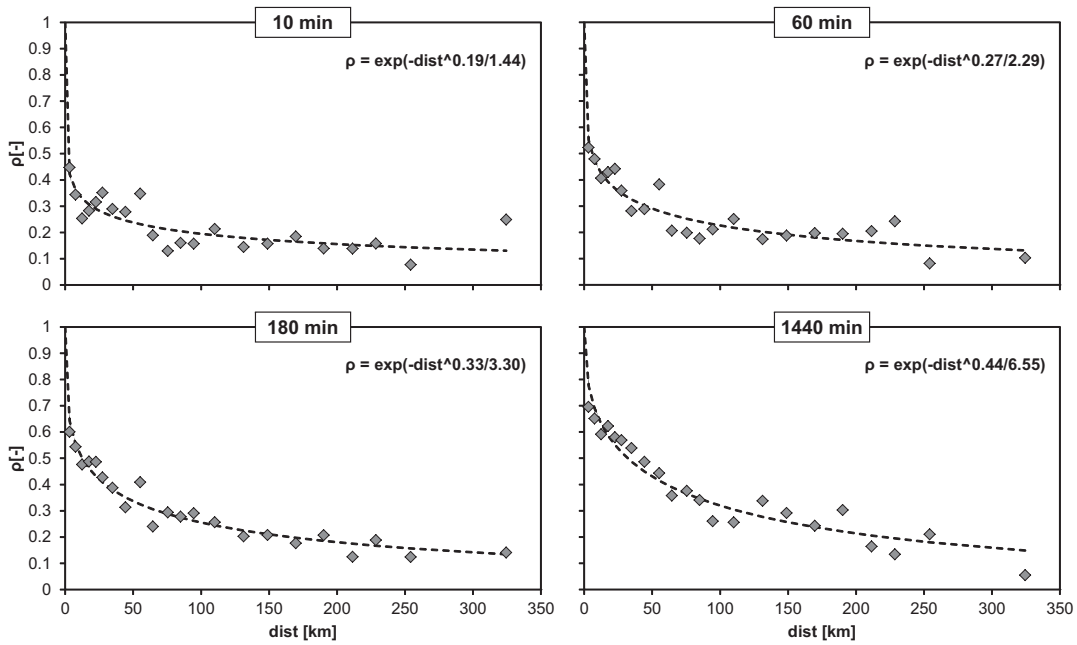
Figure 1. The correlogram for the spatial variation of z_0 for the four durations. Dots represent the observed correlation averaged in selected bins, the black line represents the fitted exponential model given in the top left of each graph.
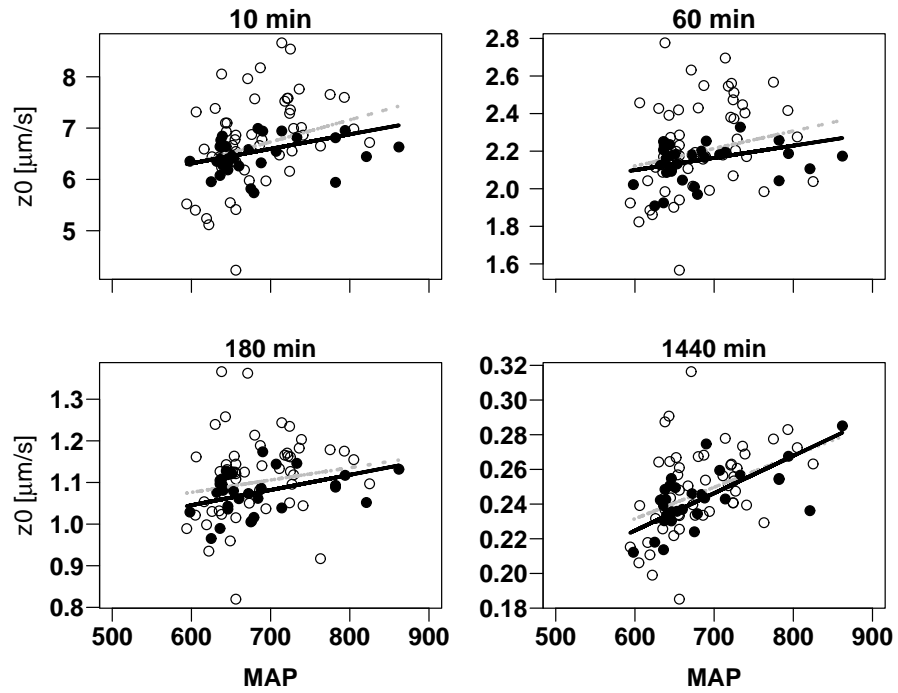
Figure 2. The OLS and GLS regression, in grey and black, respectively, showing the variation of z_0 as a function of *MAP*. The marked z_0 values are from stations with more than 30 years of observation and thereby have a high weight in the GLS model.
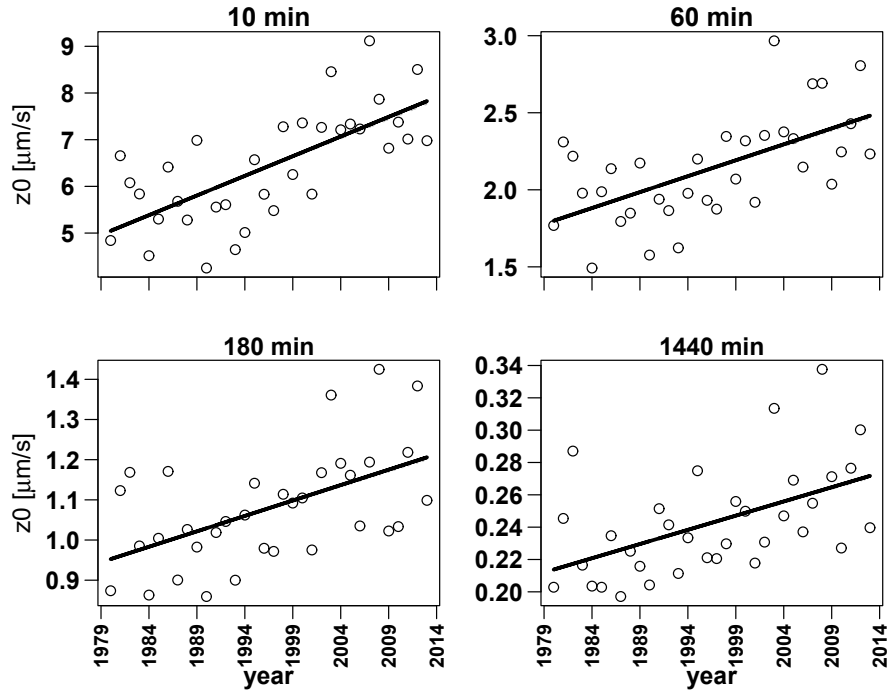
Figure 3. The OLS and GLS regression (which are identical), showing the variation of z_0 as a function of *time*.
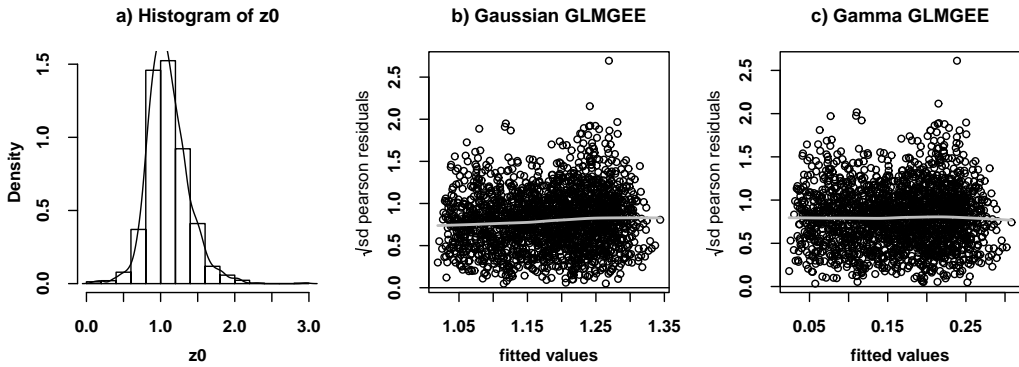

Figure 4. Evaluation of $z_{0i,s}$ to select the best underlying distribution for the GLMGEE model. b) and c) show the residuals of Eq.(18) assuming a Gaussian distribution with identity link and a Gamma distribution with log link, respectively. The graphs are for a duration of 180 minutes but similar results are obtained for the other three durations.
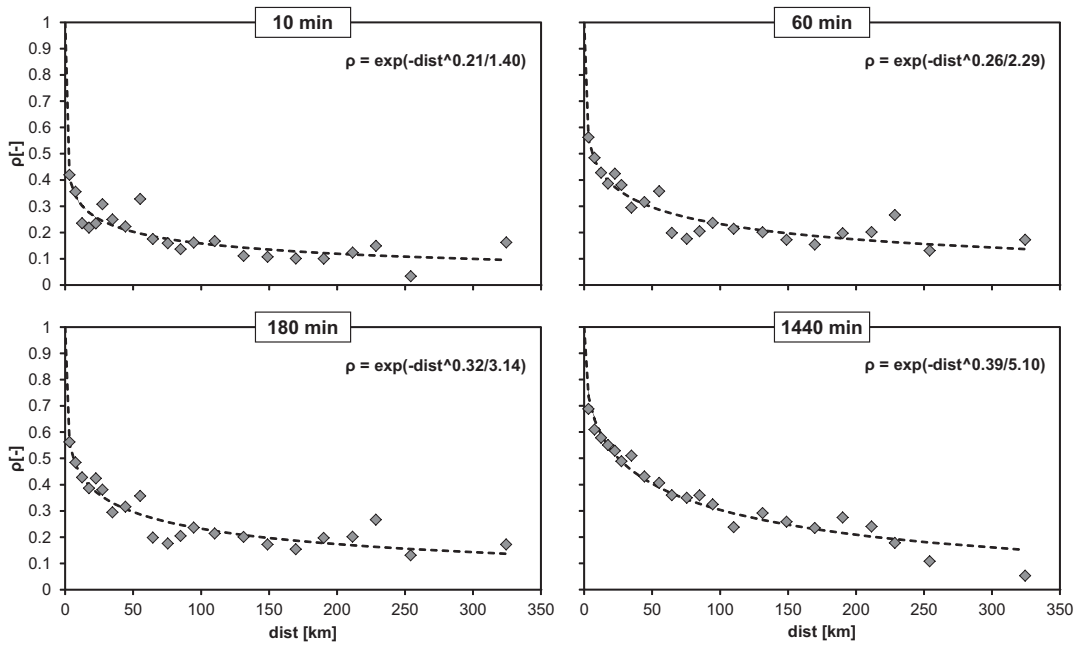
Figure 5. The correlogram for the spatial variation of λ. Blue dots represents the observed correlation averaged in selected bins, the black line represents the fitted exponential model given in the top left of each graphs.

Figure 6. The correlogram for the spatial variation of μ. Blue dots represents the observed correlation averaged in selected bins, the black line represents the fitted exponential model given in the top left of each graphs.
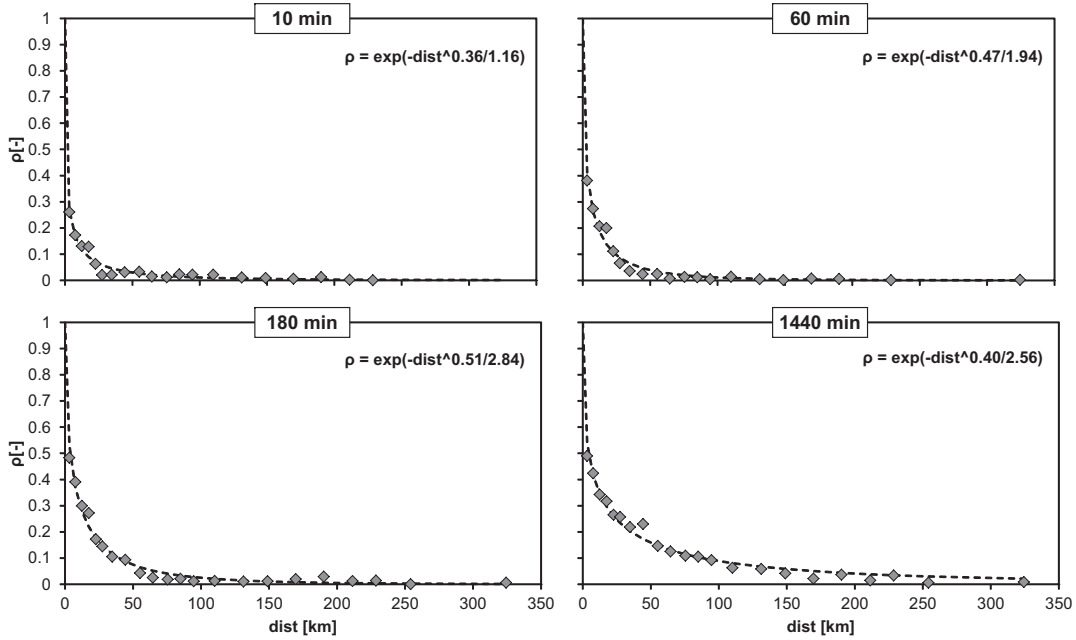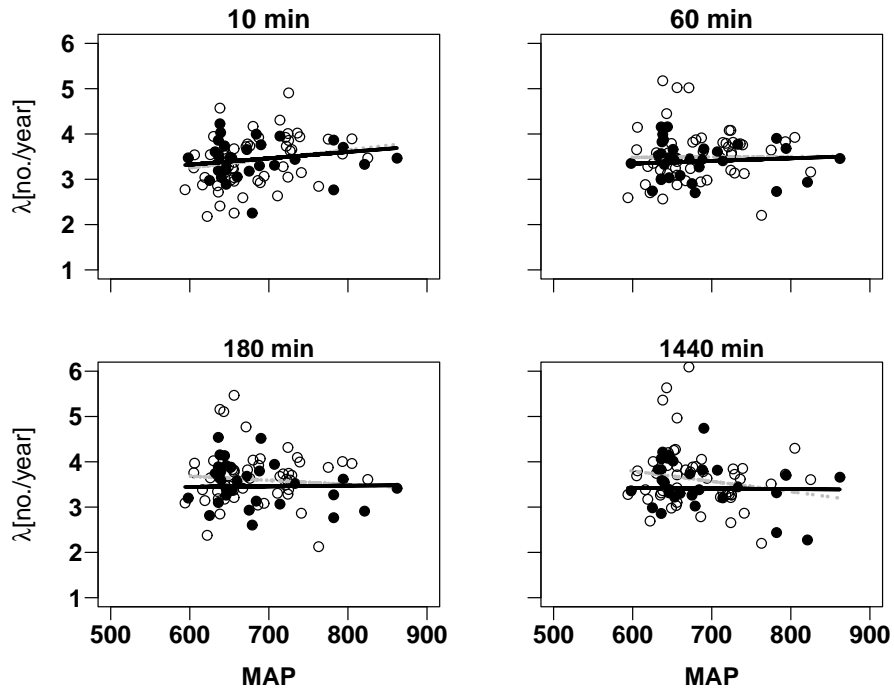
Figure 7. Marginal regional variation of λ from a PDS sampling with a spatio-temporal z_0. OLS and GLS regression are shown in grey and black, respectively. The marked λ values are from stations with more than 30 years of observation.
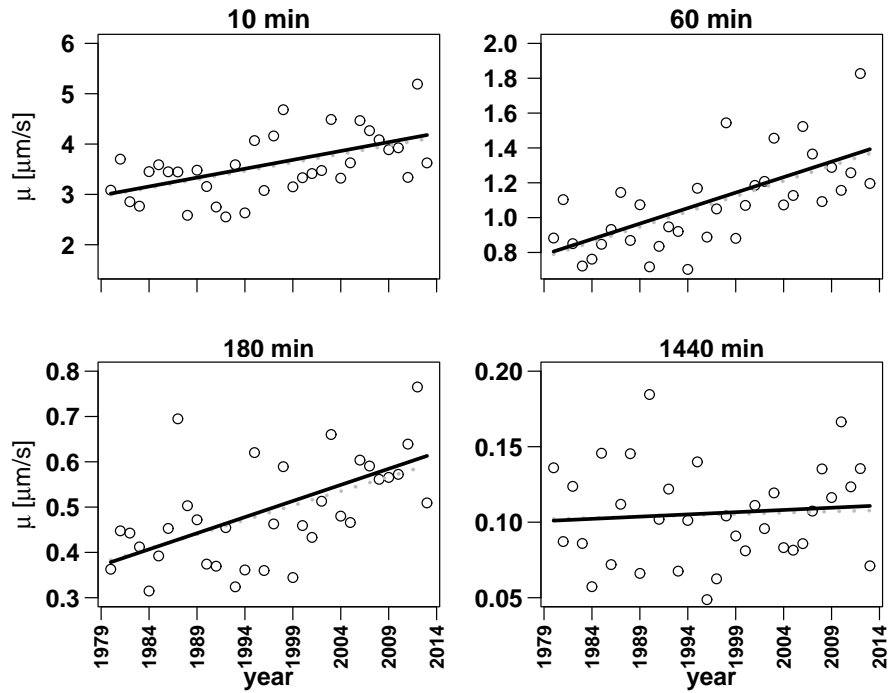
Figure 8. Marginal temporal variation of μ from a PDS sampling with a spatio-temporal z_0. OLS (grey line) and GLS (black line) regression estimates are almost identical.
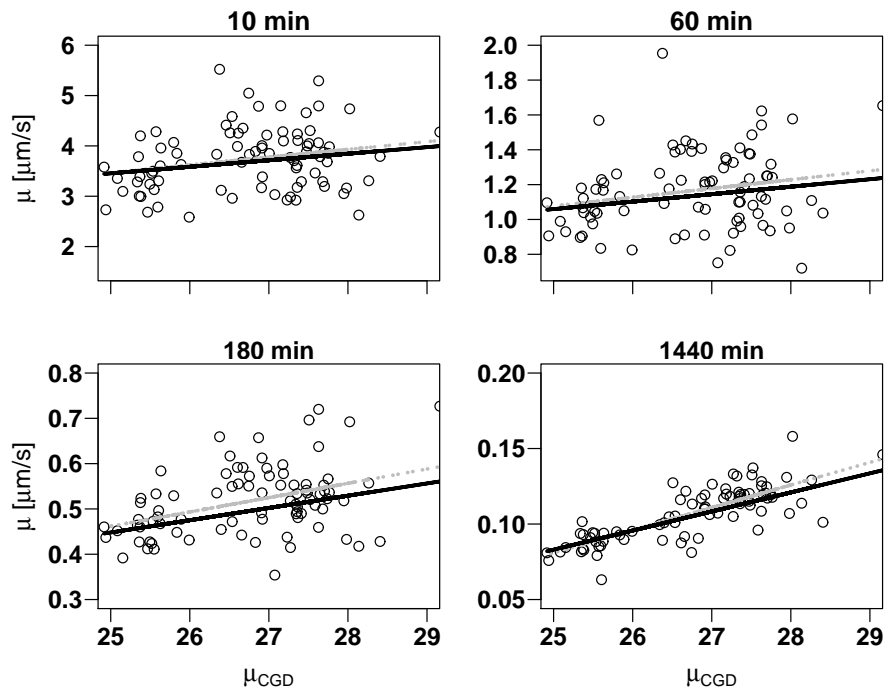

Figure 9. Marginal regional variation of μ from a PDS sampling with a spatio-temporal z_0. OLS and GLS regression are shown in grey and black, respectively.
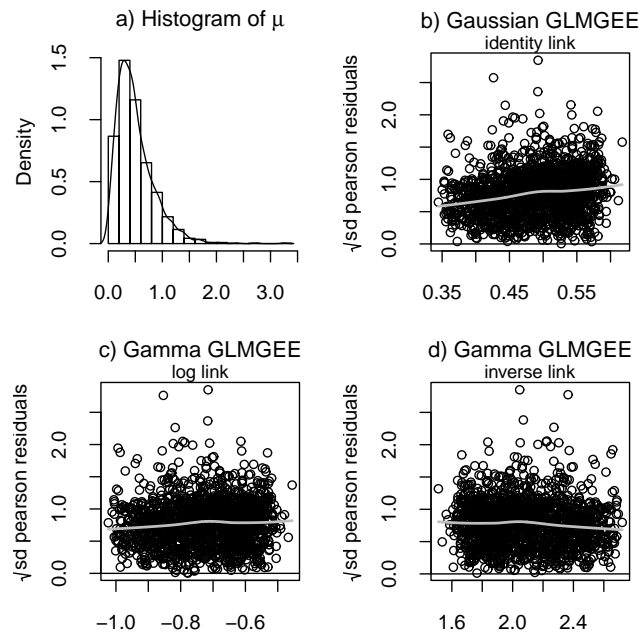
Figure 10. Evaluation of $\mu_{i,s}$ to select the best underlying distribution for the GLMGEE model. b), c) and d) show the residuals of Eq.(24) assuming a Gaussian distribution with identity link, a Gamma distribution with log link and a Gamma distribution with inverse link, respectively. The graphs are for a duration of 180 minutes.

Table 1. The estimated GLS parameters in the marginal regional regression models for z_{0s} [a]

Duration [min]	a [μm/s]	b [μm/s/mm]	p_b	$\hat{\sigma}_\delta^2$	MSE$_\varepsilon$	MSE$_\varepsilon$ reduction
10	4.61 (1.102)	0.0028 (0.0015)	0.07	0.248	0.492 (80)	9.77%
60	1.71 (0.346)	$6.5 \cdot 10^{-4}$ ($4.8 \cdot 10^{-4}$)	0.18	0.022	0.041 (80)	5.91%
180	0.83 (0.158)	$3.6 \cdot 10^{-4}$ ($2.2 \cdot 10^{-4}$)	0.10	0.0050	0.0073 (80)	3.57%
1440	0.10 (0.037)	$2.2 \cdot 10^{-4}$ ($5.2 \cdot 10^{-5}$)	<0.01	$2.8 \cdot 10^{-4}$	$3.7 \cdot 10^{-4}$ (80)	21.82%

[a] p_b measures the significance of b, which represents the regression to *MAP* [mm], see Eq.(16). MSE$_\varepsilon$ denotes the Mean Squared Error of the residuals with degrees of freedom given in parenthesis. The MSE$_\varepsilon$ reduction is estimated by comparison with an intercept model. For the regression parameters standard deviation is given in parenthesis.

Table 2. The estimated GLS parameters in the marginal temporal regression models for z_{0i} [a]

Duration [min]	a [μm/s]	c [μm/s/year]	p_c	$\hat{\sigma}_\delta^2$	MSE$_\varepsilon$	MSE$_\varepsilon$ reduction
10	4.95 (0.40)	0.085 (0.018)	<0.01	$5.4 \cdot 10^{-4}$	0.726 (31)	47.43%
60	1.78 (0.13)	0.021 (0.0059)	<0.01	$4.2 \cdot 10^{-4}$	0.073 (31)	35.07%
180	0.94 (0.060)	0.0078 (0.0027)	-	0	0.014 (31)	28.74%
1440	0.21 (0.017)	0.0018 ($7.5 \cdot 10^{-4}$)	-	0	$7.9 \cdot 10^{-4}$ (31)	26.56%

[a] p_c measures the significance of c, which represents the regression to *time* [year], see Eq.(17). MSE$_\varepsilon$ denotes the Mean Squared Error of the residuals with degrees of freedom given in parenthesis. The MSE$_\varepsilon$ reduction is estimated by comparison with an intercept model. For the regression parameters standard deviation is given in parenthesis.

Table 3. The estimated parameters in the Gaussian GLMGEE models for $z_{0i,s}$, compared to the two marginal GLS models from Table 1 and Table 2[a]

Duration [min]		a [μm/s]	b [μm/s/mm]	p_b	c [μm/s/year]	p_c	MSE_ε reduction
10	GLMGEE	3.79 (0.67)	0.0021 (0.0009)	0.02	0.080 (0.014)	<0.01	14.3%
	marginal GLS		0.0028 (0.0015)	0.07	0.085 (0.018)	<0.01	
60	GLMGEE	1.50 (0.23)	$5.3 \cdot 10^{-4}$ ($3.1 \cdot 10^{-4}$)	0.08	0.018 (0.005)	<0.01	10.0%
	marginal GLS		$6.5 \cdot 10^{-4}$ ($4.8 \cdot 10^{-4}$)	0.18	0.021 (0.0059)	0.01	
180	GLMGEE	0.72 (0.10)	$3.8 \cdot 10^{-4}$ ($1.5 \cdot 10^{-4}$)	<0.01	0.0060 (0.0018)	<0.01	7.10%
	marginal GLS		$3.6 \cdot 10^{-4}$ ($2.2 \cdot 10^{-4}$)	0.10	0.0078 (0.0027)	-	
1440	GLMGEE	0.044 (0.024)	$2.6 \cdot 10^{-4}$ ($3.0 \cdot 10^{-5}$)	<0.01	0.0013 ($4.5 \cdot 10^{-4}$)	<0.01	9.7%
	marginal GLS		$2.2 \cdot 10^{-4}$ ($5.2 \cdot 10^{-5}$)	<0.01	0.0018 ($7.5 \cdot 10^{-3}$)	-	

[a]p_b measures the significance of b, which represents the regression to *MAP* [mm], see Eq.(18). p_c measures the significance of c, which represents the regression to *time* [year], see Eq.(18). The MSE_ε reduction is estimated by comparison with an intercept model. For the regression parameters standard deviation is given in parenthesis.

Table 4. The estimated parameters in the Poisson GLMGEE models for $N_{i,s}$ with a log-link, see Eq. (21)[a]

	10 min	60 min	180 min	1440 min
a	-4.65	-4.63	-4.60	-4.62
	(0.048)	(0.054)	(0.052)	(0.055)
scale of Poisson	1.22	1.26	1.23	1.15
λ [no./year]	3.48	3.56	3.67	3.58
	(0.17)	(0.19)	(0.19)	(0.20)

[a]a represents the model intercept, see Eq.(21). The scale measures the dispersion of the Poisson distribution, see *Gregersen et al.* [2013a]. λ is predicted from the model using an observation period of one year ($l_{i,s}$ = 365 days). Uncertainty on the estimates is given in parenthesis.

Table 5. The estimated parameters in the Gamma GLMGEE models for $\mu_{0i,s}$, compared to the two marginal GLS models[a]

Duration [min]		a	b	p_b	c	p_c	Gamma scale	MSE_ε reduction
10	GLMGEE	0.51 (0.19)	$-7.0\cdot10^{-3}$ ($7.1\cdot10^{-3}$)	0.32	$-2.4\cdot10^{-3}$ ($5.8\cdot10^{-4}$)	<0.01	0.49	
	marginal GLS		0.13 (0.079)	0.10	0.035 ($9.8\cdot10^{-3}$)	<0.01		
	reduced GLMGEE	0.32 (0.016)			$-2.4\cdot10^{-3}$ ($5.8\cdot10^{-4}$)	<0.01	0.49	3.07%
60	GLMGEE	1.24 (0.64)	-0.020 (0.024)	0.93	-0.014 ($2.6\cdot10^{-3}$)	<0.01	0.53	
	marginal GLS		0.043 (0.031)	0.17	0.018 ($3.7\cdot10^{-3}$)	<0.01		
	reduced GLMGEE	1.19 (0.064)			-0.014 ($2.6\cdot10^{-3}$)	<0.01	0.53	9.64%
180	GLMGEE	4.83 (1.32)	-0.084 (0.051)	0.10	-0.026 ($6.0\cdot10^{-3}$)	<0.01	0.49	7.99%
	marginal GLS		0.027 (0.012)	0.02	$7.1\cdot10^{-3}$ ($1.7\cdot10^{-3}$)	<0.01		
	reduced GLMGEE	2.61 (0.15)			-0.026 ($5.9\cdot10^{-3}$)	<0.01	0.50	5.64%
1440	GLMGEE	47.77 (7.76)	-1.39 (0.29)	<0.01	-0.019 (0.052)	0.71	0.53	
	marginal GLS		0.013 ($2.6\cdot10^{-3}$)	<0.01	$2.9\cdot10^{-4}$ ($5.6\cdot10^{-4}$)	0.60		
	reduced GLMGEE	47.65 (7.79)	-1.40 (0.30)	<0.01			0.53	17.8%

[a]Due to the inverse link function of the GLMGEE model, parameters cannot be directly compared but the significance can. In the reduced GLMGEE non-significant terms have been excluded. Uncertainty on the parameter estimates is given in parenthesis. MSE_ε denotes the Mean Squared Error of the residuals. The MSE_ε reduction is estimated by comparison with an intercept model.

Table 6. Estimations of L_{cv} and κ[a]

	10 min	60 min	180 min	1440 min
L_{cv}	0.53 ($7.1 \cdot 10^{-5}$)	0.55 ($2.7 \cdot 10^{-4}$)	0.54 ($4.0 \cdot 10^{-4}$)	0.54 ($1.5 \cdot 10^{-4}$)
κ	-0.12 ($8.8 \cdot 10^{-4}$)	-0.19 ($2.9 \cdot 10^{-3}$)	-0.16 ($4.6 \cdot 10^{-3}$)	-0.15 ($1.8 \cdot 10^{-3}$)

[a]Uncertainty on the parameter estimates is given in parenthesis.

Table 7. Estimations of design intensities with a return period of 10 years, uncertainty is given in parenthesis[a]

	MAP [mm]	μ_{CGD} [mm]	10 min [µm/s]	60 min [µm/s]	180 min [µm/s]	1440 min [µm/s]
Madsen *et al.* (in prep)	707	25.5	21.30 (1.83)	6.91 (0.94)	2.99 (0.35)	0.61 (0.052)
Eq.(25) with i=1996	707	25.5	20.00 (0.90)	6.59 (0.50)	2.93 (0.26)	0.59 (0.032)
Eq.(25) with i=2005	707	25.5	21.90 (0.97)	7.42 (0.58)	3.20 (0.29)	0.60 (0.032)
Madsen *et al.* (in prep)	660	27.4	20.99 (1.81)	6.84 (0.93)	3.21 (0.38)	0.69 (0.062)
Eq.(25) with i=1996	660	27.4	19.93 (0.90)	6.57 (0.50)	3.05 (0.28)	0.68 (0.045)
Eq.(25) with i=2005	660	27.4	21.84 (0.97)	7.39 (0.58)	3.36 (0.31)	0.69 (0.045)

[a]The selected locations correspond to the two largest cities in Denmark (Aarhus and Copenhagen).